is a binary label, $\boldsymbol{x}$ is the input vector (coding neural activity), and $f(\boldsymbol{x})$ is a linear function of the form $f(\boldsymbol{x}) = \boldsymbol{w} \cdot \boldsymbol{x} + b = \sum_i^m c_i(\boldsymbol{x} \cdot \boldsymbol{x}_i) + b$. Training means estimating the vector of coefficients $\boldsymbol{w}$ and the scalar b from the training set of m $(\boldsymbol{x}_i, y_i)$ pairs, where $\boldsymbol{x}_i$ is the "input" part of each example and y_i is its associated label or "output." More complex classifiers of the form $f(\boldsymbol{x}) = \sum_i^m c_i k(\boldsymbol{x}, \boldsymbol{x}_i)$ had very similar performance and were no better than the regularized linear classifiers for $n > 64$ sites. The estimated coefficients depend on regularization and are different for different regularization techniques (*21*).

35. Multiple sources of noise can affect the encoding of information. The performance of the classifier was very robust to deletions of substantial numbers of neurons during testing, simulating neuronal or synaptic death (fig. S1A), and also to large proportions of deleted spikes (simulating failures in spike transmission or neurotransmitter release; fig. S1B).
36. We trained the classifier for the categorization task with 70% of the pictures and then tested it on the remaining 30% of the pictures. The performance was quite good and only slightly below the performance levels reported above (fig. S3; compare to Fig. 1).
37. Y. Sugase, S. Yamane, S. Ueno, K. Kawano, *Nature* **400**, 869 (1999).
38. R. Vogels, *Eur. J. Neurosci.* **11**, 1239 (1999).
39. B. Tjan, *Adv. Neural Inf. Processing Syst.* **13**, 66 (2001).
40. T. Poggio, E. Bizzi, *Nature* **431**, 768 (2004).
41. N. C. Aggelopoulos, L. Franco, E. T. Rolls, *J. Neurophysiol.* **93**, 1342 (2005).
42. We thank M. Kouh for the object recognition model; R. Quiroga and A. Kraskov for spike sorting; J. Mayo and J. Deutsch for technical support; CSBI for computer cluster usage; and R. Desimone, N. Kanwisher, C. Koch, and T. Serre for comments on the manuscript. This research was sponsored by grants from NIH, NSF, and especially from the Defense Advanced Research Projects Agency and Office of Naval Research. Additional support was provided by Eastman Kodak Company, Daimler Chrysler, Honda Research Institute, The Pew Charitable Trusts, Whiteman fellowship (G.K.), and the McDermott chair (T.P.).

Supporting Online Material
www.sciencemag.org/cgi/content/full/310/5749/863/DC1
SOM Text
Figs. S1 to S7
References

19 July 2005; accepted 5 October 2005
10.1126/science.1117593

Neuronal Activity Regulates Diffusion Across the Neck of Dendritic Spines

Brenda L. Bloodgood and Bernardo L. Sabatini*

In mammalian excitatory neurons, dendritic spines are separated from dendrites by thin necks. Diffusion across the neck limits the chemical and electrical isolation of each spine. We found that spine/dendrite diffusional coupling is heterogeneous and uncovered a class of diffusionally isolated spines. The barrier to diffusion posed by the neck and the number of diffusionally isolated spines is bidirectionally regulated by neuronal activity. Furthermore, coincident synaptic activation and postsynaptic action potentials rapidly restrict diffusion across the neck. The regulation of diffusional coupling provides a possible mechanism for determining the amplitude of postsynaptic potentials and the accumulation of plasticity-inducing molecules within the spine head.

In mammalian excitatory neurons, synaptic stimulation triggers the flow of ions across the dendritic spine membrane, as well as the production of second messengers within the spine head. Buildup of signaling molecules, such as calcium or activated CaMKII (calcium/calmodulin-dependent protein kinase II), within the spine head activates regulatory cascades that lead to the modification of the enclosed synapse (*1*–*4*). Furthermore, stimulus-induced transport of proteins across the spine neck, such as CaMKII, protein translation initiation factors, and β-catenin, plays a role in synapse regulation and plasticity (*5*, *6*). Thus, the regulation of diffusion across the spine neck offers a potentially powerful mechanism to control the efficacy and modulatory state of individual synapses.

We examined the regulation of the diffusional barrier posed by spine necks in rat hippocampal pyramidal neurons. Organotypic slice cultures were biolistically transfected with the photoactivatable green fluorophore PAGFP (*7*) and the red fluorophore dsRed. Two-photon laser scanning microscopy (2PLSM) with illumination at 910 nm readily excites dsRed without photoactivation of PAGFP, revealing dendrites and spines that fluoresce in the red spectrum (Fig. 1). Focal illumination with a second laser tuned to 720 nm triggers two-photon activation of PAGFP (*8*), and the resulting green fluorescence can be subsequently monitored with 910-nm illumination. Photoactivation of PAGFP within individual spines triggers increases in fluorescence within the head that dissipate as activated PAGFP (PAGFP*) diffuses into the dendrite. The decay of the fluorescence transient in the spine head is well fit by a single exponential, yielding a time constant of equilibration (τ_{equ}) (*9*) of PAGFP* across the spine neck (Fig. 1, A to C). Repeated measurements (at 0.1 Hz) in individual spines over ~1.5 min yielded consistent values of τ_{equ} (fig. S1) with coefficients of variation (CVs) of ~15 to 20% (Fig. 1D). Conversely, τ_{equ} varied over a broad range from spine to spine (Fig. 1E, n = 11/572 cells/spines), with the majority of values ranging from 140 to 350 ms.

In a subset of spines, fluorescence did not decay appreciably in the sampling period of 1.9 s. For these spines, the barrier to PAGFP* movement across the neck was bidirectional, so that PAGFP* within the dendrite is able to diffuse away from the site of photoactivation but does not enter the spine head (Fig. 2, A and B; similar findings in 11 of 11 comparable spine/dendrite pairs). Conversely, PAGFP* diffuses from the dendrite into the heads of spines with less restrictive spine necks (Fig. 2, C and D; similar findings in 8 of 8 comparable spine/dendrite pairs). Thus, the lack of PAGFP* movement in a subset of spines results from a severe diffusional isolation imposed by the spine neck and not from aggregation or cross-linking of PAGFP within the head. Repeated measurements of τ_{equ} in these diffusionally isolated spines over prolonged periods revealed that the diffusional barrier is reversible and that large, apparently spontaneous reductions in τ_{equ} occur (Fig. 2, E and F; similar findings in 4 of 15 diffusionally isolated spines that were monitored repeatedly for >5 min).

We hypothesized that the heterogeneity of τ_{equ} results from active regulation of diffusional coupling in response to variability in neuronal and synaptic activity. Chronic manipulations of activity trigger homeostatic changes in synaptic parameters such as the number and composition of AMPA-type glutamate receptors (AMPARs) at the synapse (*10*, *11*). Consistent with our hypothesis, 24 hours of incubation in the AMPAR antagonist NBQX shifted the distribution of τ_{equ} toward faster values (8/367 cells/spines; $P < 0.01$), whereas block of $GABA_A$ receptors ($GABA_A$Rs) with bicuculline shifted the distribution toward slower values (8/556 cells/spines; $P < 0.01$) (Fig. 3A). Similar results were obtained with measurements of dsRed diffusion by fluorescence recovery after photobleaching (fig. S2). In contrast, block of voltage-sensitive sodium channels (VSSCs) (6/438 cells/spines) or NMDA-type glutamate receptors (NMDARs) (7/449 cells/spines) by incubation in tetrodotoxin (TTX) or carboxypiperazin-4-yl-propyl-1-phosphonic acid (CPP), respectively, had no effect on the cumulative distribution of τ_{equ}

Department of Neurobiology, Harvard Medical School, 220 Longwood Avenue, Boston, MA 02115, USA.

*To whom correspondence should be addressed. E-mail: bsabatini@hms.harvard.edu

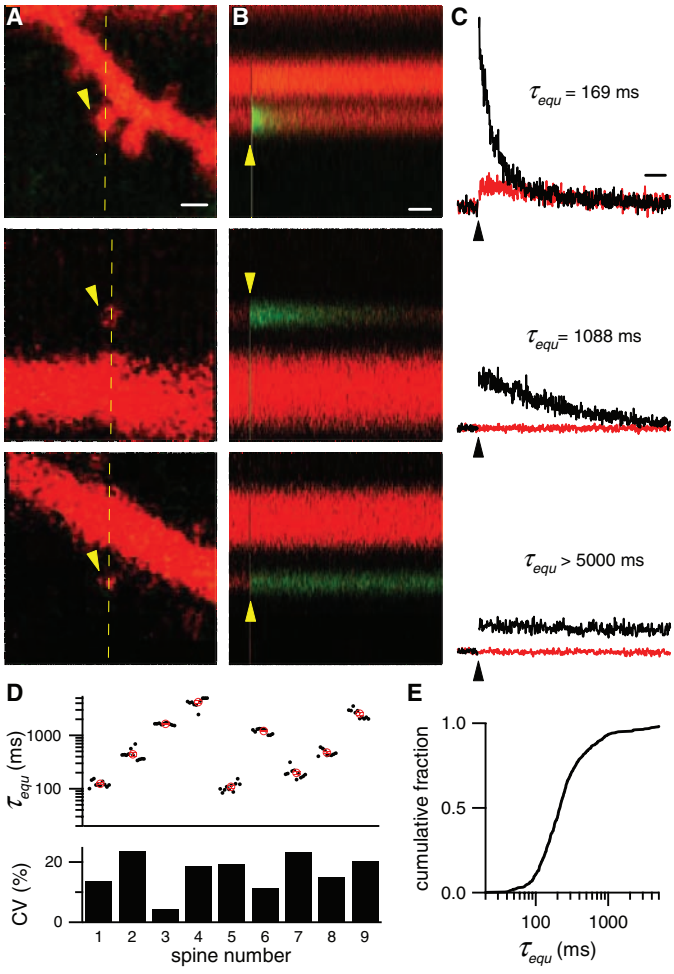

Fig. 1. Measurement of PAGFP* movement across the spine neck reveals heterogeneity of spine/dendrite diffusional coupling. (**A**) Images of spine/dendrite pairs that demonstrate strong (top), moderate (middle), and weak (bottom) diffusional coupling. In (A) to (C), the arrowhead indicates the site of photoactivation. Scale bar, 1 μm. (**B**) Fluorescence measured in line scans over the regions indicated by the dashed lines in (A) during photoactivation of PAGFP in the spine head. Scale bar, 200 ms. (**C**) Quantification of the PAGFP* fluorescence transients in the spine head (black) and dendrite (red) shown in (B). Scale bar, 200 ms. (**D**) Repeated measurements of τ_{equ} in each of nine spines (top). For each spine, the values of τ_{equ} obtained from each independent measurement (black points), the average ± SEM (red), and the CV of τ_{equ} (bottom) are shown. (**E**) Cumulative distribution of τ_{equ} for spines in control conditions.

(Fig. 3A). However, all manipulations altered the fraction of highly diffusionally isolated spines (f_{slow}), defined here as those with τ_{equ} > 2000 ms. Reducing activity levels by incubation in TTX, CPP, or NBQX decreased f_{slow} to 1.6, 1.9, and 1.8%, respectively, whereas increasing activity by block of inhibition with bicuculline increased f_{slow} to 16.4% ($P < 0.01$ for each condition compared to f_{slow} = 4.9% in control conditions, Fig. 3B). To determine whether increases in τ_{equ} are a direct consequence of blocking $GABA_AR$ signaling or are triggered by the increased action potential (AP) firing that results from the removal of inhibition, τ_{equ} was measured after incubation in the presence of both $GABA_AR$ and VSSC blockers (bicuculline and TTX). In these conditions, the distribution of τ_{equ} and the value of f_{slow} (f_{slow} = 2.0%) were the same as in the presence of TTX alone (*12*), suggesting that the loss of spontaneous $GABA_A$ currents is not sufficient to trigger modification of τ_{equ} and that secondary changes in the rate of APs or glutamatergic transmission are necessary.

τ_{equ} is determined by several factors such that $\tau_{equ} = VL/DA$, where V is the volume of the spine head, L is the length of the spine neck, D is the diffusion coefficient of the molecule, and A is the cross-sectional area of the spine neck (*9*). Regulation of any of these parameters might account for the observed changes in τ_{equ}. Each pharmacological manipulation had differential effects on the distributions of head widths and neck lengths (Fig. 3C and fig. S3). However, comparison of diffusional coupling across conditions for spines of similar morphology indicates that these alterations do not explain the observed

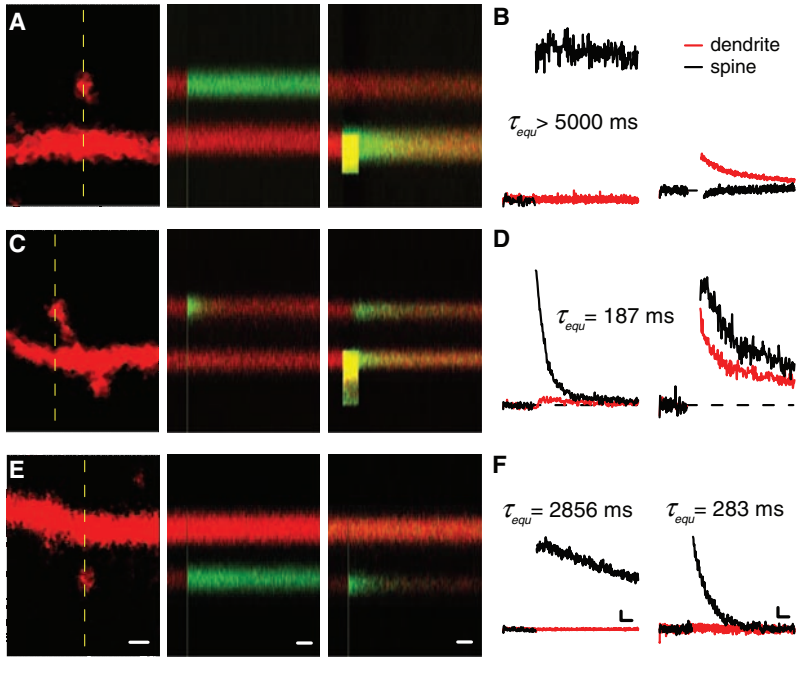

Fig. 2. The spine neck is a bidirectional and dynamic barrier to protein movement. (**A**) Image of spine/dendrite pair (left) demonstrating weak diffusional coupling and fluorescence transients obtained after photoactivation in the spine head (middle) or neighboring dendrite (right). (**B**) Quantification of the spine (black) and dendrite (red) fluorescence transients from the corresponding panels in (A) (middle and right). (**C**) Image of spine/dendrite pair (left) demonstrating strong diffusional coupling and fluorescence transients obtained after photoactivation in the spine head (middle) or neighboring dendrite (right). (**D**) Quantification of the spine (black) and dendrite (red) fluorescence transients from the corresponding panels in (C) (middle and right). (**E**) Image of spine/dendrite pair that switches from weak to strong diffusional coupling (left). Diffusional coupling was initially weak (middle) but spontaneously switched to strong (right) several minutes later. (**F**) Quantification of the spine (black) and dendrite (red) fluorescence transients from the corresponding panels in (E) (middle and right). Scale bars, 1 μm (left) and 200 ms (right and middle) for (A), (C), and (E); 10% ΔG/R and 200 ms for (B), (D), and (F).

changes in τ_{equ}. After $GABA_AR$ blockade, τ_{equ} was significantly larger than for control spines of matched neck length or apparent head width (Fig. 3D). Conversely, after AMPAR blockade, spines tended toward faster τ_{equ} than control spines with comparable morphology. Furthermore, spine neck lengths were reduced equally after NMDAR or AMPAR blockade (fig. S3), but only in the latter condition was the distribution of τ_{equ} shifted to faster values.

To determine whether cell-wide changes in cytoplasmic viscosity account for the changes in τ_{equ}, the diffusion coefficient of PAGFP* (D_{PAGFP*}) was measured in aspiny regions of thin (~1 to 2 μm in diameter) dendrites. D_{PAGFP*} (37 ± 10 μm²/s in control conditions) was consistent with previous measurements of green fluorescent protein (GFP) motility (*13*) and was constant across pharmacological conditions (fig. S4), indicating that the movement of proteins across the neck is specifically regulated in response to the manipulations of activity. Thus, changes in V, L, or D_{PAGFP*} do not account for the effects of activity on spine/dendrite diffusional coupling, suggesting that the cross-sectional area of the neck is the regulated parameter. This regulation may result from active constriction of the spine neck. Alternatively, the accessible cross-sectional area of the neck may change because of rearrangement of the cytoskeleton or the movement of organelles into the neck (*14–17*).

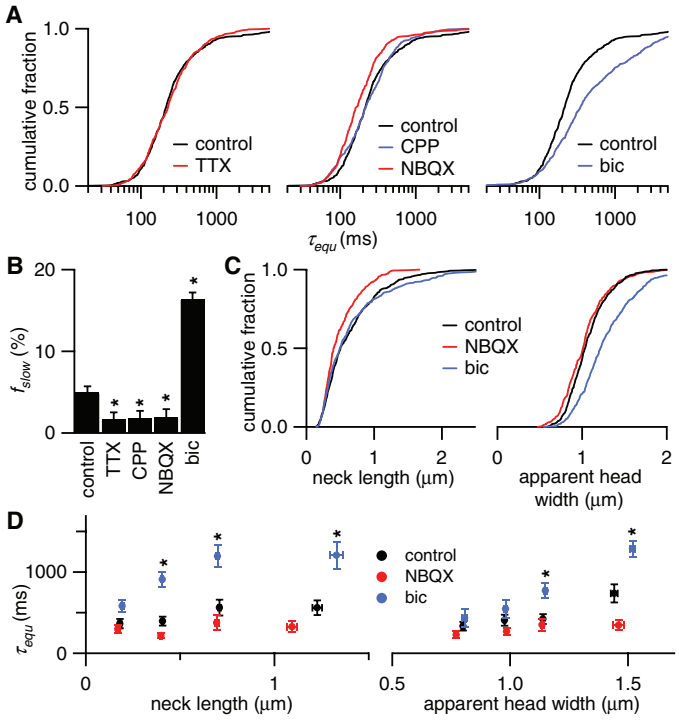

Fig. 3. The diffusional barrier posed by the spine neck is regulated by activity. (**A**) The overall distribution of τ_{equ} is unchanged when action potentials (TTX, left) or NMDAR (CPP, middle) are blocked. Blocking AMPAR (NBQX, middle) significantly decreases τ_{equ}, whereas blocking $GABA_AR$ increases τ_{equ} [bicuculline (bic), right]. (**B**) Reducing activity with TTX, CPP, or NBQX reduces the fraction of diffusionally isolated spines (f_{slow}), whereas increasing activity with bicuculline increases f_{slow}. Asterisks indicate $P < 0.01$ relative to control. (**C**) Cumulative distribution of measured neck length and apparent head width in control, NBQX-, or bicuculline-treated cultures. (**D**) Average τ_{equ} calculated for spines of similar neck lengths (left) or head widths (right) in control, NBQX-, and bicuculline-treated cultures. Asterisks indicate $P < 0.01$ relative to control.

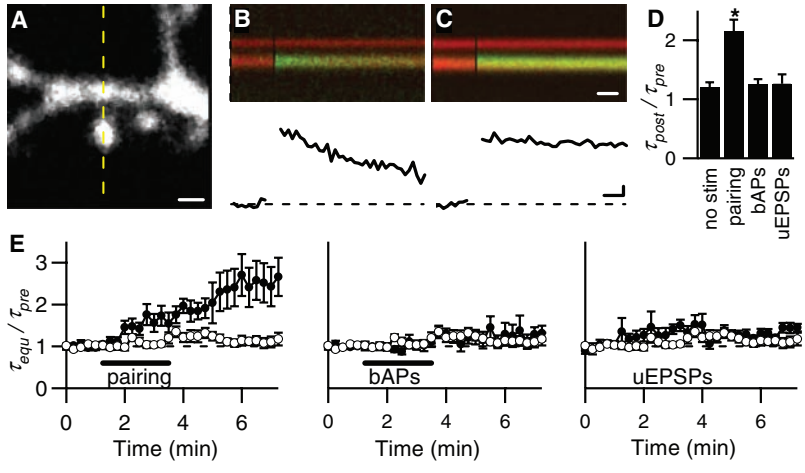

Fig. 4. Diffusion across the spine neck is restricted in response to pairing of synaptic potentials and bAPs. (**A**) Image of spiny dendrite of a neuron filled with Alexa Fluor-594 and NPE-HPTS. The dashed line indicates the orientation of the line scan used in (B) and (C). Scale bar, 1 μm. (**B**) Average line scan fluorescence transients (top) and the quantification of the fluorescence transient in the spine head (bottom) after photoactivation in the spine head in the baseline period. (**C**) As in (B), for data collected after 10 consecutive pairings of uEPSPs and bAPs. Scale bars, 10% ΔG/R and 50 ms for (B) and (C). (**D**) Fractional change in τ_{equ} after imaging alone, pairing of uEPSPs and bAPs, or stimulation with bAPs or uEPSPs alone. (**E**) Time course of fractional changes in τ_{equ} triggered by imaging alone (open circles) or stimulation (solid circles) with paired uEPSPs and bAPs (left), bAPs alone (middle), or uEPSPs alone (right).

Is diffusional equilibration across the spine neck also regulated acutely by the activity of the synapse enclosed in the spine head? The effects of back-propagating action potentials (bAPs), synaptic activity, and the pairing of bAPs with synaptic activity on the spine neck diffusional resistance (Fig. 4) were measured. For these experiments, spine/dendrite diffusional coupling was measured by photoactivation of NPE-HPTS, a caged version of the green-fluorescing, pyranine-based fluorophore HPTS (*18*). Whole-cell–current clamp recordings were obtained from hippocampal pyramidal neurons that were filled through the patch pipette with NPE-HPTS and Alexa Fluor-594 and bathed in 5 mM MNI-glutamate, a caged version of glutamate (*19*). Illumination at 720 nm for 0.5 ms was used to photoactivate NPE-HPTS and uncage glutamate, and the laser power was set to generate fluorescence transients of ~20%, a 20% increase in green fluorescence relative to the resting red fluorescence (ΔG/R) in the spine head. Pairing of uncaging-evoked EPSPs (uEPSPs) with small bursts of bAPs (3 bAPs at 50 Hz) triggered increases in τ_{equ} that continued after the end of the pairing period (Fig. 4E) ($n = 8/12$ cells/spines, $P < 0.05$). In contrast, bAPs ($n = 8/9$) or uEPSPs ($n = 6/11$) alone, as well as repeated monitoring of τ_{equ} without stimulation ($n = 6/11$), had no effect on τ_{equ}. For all four experimental conditions (uEPSP/bAP pairing, uEPSPs alone, bAPs alone, and no stimulation), the analyzed spine experienced identical photoactivation and imaging laser exposures. Thus, the restriction of diffusion across the spine neck seen in response to the pairing of bAPs and synaptic stimulation represents a cellular response to the stimulus. Furthermore, because HPTS is a small polar molecule, its diffusion is similar to that of second messengers such as cyclic adenosine monophosphate.

The regulation of spine/dendrite diffusional equilibration may have several functional consequences. First, the susceptibility of individual synapses to plasticity induction

may be influenced by the ability of signaling molecules to move into and out of the spine head. Synaptic plasticity is typically induced by either repetitive low-frequency stimulation (*20*–*23*) or by ~1-s bursts of high-frequency stimulation (*3*, *24*, *25*) during which the spine must integrate biochemical signals. Spines with fast diffusional equilibration across the spine neck may be unable to retain second messengers or activated proteins during the interstimulus interval. Conversely, if diffusional equilibration is slow, biochemical signals generated by synaptic activation may persist in the spine head and summate during repetitive stimulation. Second messengers and many proteins involved in spine and synapse regulation are similar in size to HPTS (~500 daltons) and PAGFP (28 kD), respectively, and will experience similar diffusional barriers at the spine neck. Thus, the regulation of diffusion across the spine neck in response to changes in the activity patterns of individual cells and synapses may serve to set the threshold for plasticity induction. Second, previous estimates of diffusional coupling indicated that the barrier posed by the neck was too small to allow for a substantial voltage drop across the neck after synaptic activation of glutamate receptors (*9*). This reinforced the notion that spines function as biochemical and not electrical signaling compartments (*26*). However, the diffusionally isolated spines uncovered here have τ_{equ} approximately 10-fold greater than the population mean, suggesting a spine neck resistance approaching 1 gigohm (*9*). The stimulation of synapses housed in spines with such restrictive necks may result in depolarizations and regenerative electrical signals that are confined to the spine head (*27*).

References and Notes

1. R. C. Malenka, M. F. Bear, *Neuron* **44**, 5 (2004).
2. R. J. Colbran, A. M. Brown, *Curr. Opin. Neurobiol.* **14**, 318 (2004).
3. R. Malinow, H. Schulman, R. W. Tsien, *Science* **245**, 862 (1989).
4. R. S. Zucker, *Curr. Opin. Neurobiol.* **9**, 305 (1999).
5. K. Shen, M. N. Teruel, J. H. Connor, S. Shenolikar, T. Meyer, *Nat. Neurosci.* **3**, 881 (2000).
6. S. Murase, E. Mosser, E. M. Schuman, *Neuron* **35**, 91 (2002).
7. G. H. Patterson, J. Lippincott-Schwartz, *Science* **297**, 1873 (2002).
8. J. N. Post, K. A. Lidke, B. Rieger, D. J. Arndt-Jovin, *FEBS Lett.* **579**, 325 (2005).
9. K. Svoboda, D. W. Tank, W. Denk, *Science* **272**, 716 (1996).
10. G. G. Turrigiano, K. R. Leslie, N. S. Desai, L. C. Rutherford, S. B. Nelson, *Nature* **391**, 892 (1998).
11. T. C. Thiagarajan, E. S. Piedras-Renteria, R. W. Tsien, *Neuron* **36**, 1103 (2002).
12. B. L. Bloodgood, B. L. Sabatini, data not shown.
13. R. Swaminathan, C. P. Hoang, A. S. Verkman, *Biophys. J.* **72**, 1900 (1997).
14. E. N. Star, D. J. Kwiatkowski, V. N. Murthy, *Nat. Neurosci.* **5**, 239 (2002).
15. M. Fischer, S. Kaech, U. Wagner, H. Brinkhaus, A. Matus, *Nat. Neurosci.* **3**, 887 (2000).
16. F. Capani, M. E. Martone, T. J. Deerinck, M. H. Ellisman, *J. Comp. Neurol.* **435**, 156 (2001).
17. Z. Li, K.-I. Okamoto, Y. Hayashi, M. Sheng, *Cell* **119**, 873 (2004).
18. N. I. Kiskin, R. Chillingworth, J. A. McCray, D. Piston, D. Ogden, *Eur. Biophys. J.* **30**, 588 (2002).
19. M. Canepari, L. Nelson, G. Papageorgiou, J. E. Corrie, D. Ogden, *J. Neurosci. Methods* **112**, 29 (2001).
20. D. E. Feldman, *Neuron* **27**, 45 (2000).
21. R. C. Froemke, M.-m. Poo, Y. Dan, *Nature* **434**, 221 (2005).
22. G.-q. Bi, M.-m. Poo, *J. Neurosci.* **18**, 10464 (1998).
23. S. M. Dudek, M. F. Bear, *J. Neurosci.* **13**, 2910 (1993).
24. T. V. Bliss, T. Lomo, *J. Physiol.* **232**, 331 (1973).
25. B. K. Andrasfalvy, J. C. Magee, *J. Physiol.* **559**, 543 (2004).
26. C. Koch, A. Zador, *J. Neurosci.* **13**, 413 (1993).
27. I. Segev, W. Rall, *J. Neurophysiol.* **60**, 499 (1988).

28. We thank members of the Sabatini lab and B. Datta for helpful comments, suggestions, and critical reading of the manuscript. We thank J. Lippincott-Schwartz and J. Corrie and D. Ogden for the generous gifts of PAGFP and NPE-HPTS, respectively. This work was funded by the Searle Scholars Program, a McKnight Technological Innovations Award, the Hellman Family Faculty Fund, and the Whitaker Foundation. The authors declare that they have no competing financial interests.

Supporting Online Material

www.sciencemag.org/cgi/content/full/310/5749/866/DC1
Materials and Methods
Figs. S1 to S4
References

13 May 2005; accepted 4 October 2005
10.1126/science.1114816

Tissue-Specific TAFs Counteract Polycomb to Turn on Terminal Differentiation

Xin Chen, Mark Hiller,* Yasemin Sancak,† Margaret T. Fuller‡

Polycomb transcriptional silencing machinery is implicated in the maintenance of precursor fates, but how this repression is reversed to allow cell differentiation is unknown. Here we show that testis-specific TAF (TBP-associated factor) homologs required for terminal differentiation of male germ cells may activate target gene expression in part by counteracting repression by *Polycomb*. Chromatin immunoprecipitation revealed that testis TAFs bind to target promoters, reduce Polycomb binding, and promote local accumulation of H3K4me3, a mark of Trithorax action. Testis TAFs also promoted relocalization of Polycomb Repression Complex 1 components to the nucleolus in spermatocytes, implicating subnuclear architecture in the regulation of terminal differentiation.

Male germ cells differentiate from adult stem cell precursors, first proliferating as spermatogonia, then converting to spermatocytes, which initiate a dramatic, cell type–specific transcription program. In *Drosophila*, five testis-specific TAF homologs (tTAFs) encoded by the *can*, *sa*, *mia*, *nht*, and *rye* genes are required for meiotic cell cycle progression (*1*, *2*) and normal levels of expression in spermatocytes of target genes involved in postmeiotic spermatid differentiation (*3*). Requirement for the tTAFs is gene selective: Many genes are transcribed normally in *tTAF* mutant spermatocytes. Tissue-specific TAFs have also been implicated in gametogenesis and differentiation of specific cell types in mammals (*4*, *5*). In addition to action with TBP (TATA box–binding protein) in TFIID, certain TAFs associate with HAT (histone acetyltransferase) or Polycomb group (PcG) transcriptional regulatory complexes (*6*, *7*). To elucidate how tissue-specific TAFs can regulate gene-selective transcription programs during development, we investigated the mechanism of action of the *Drosophila* tTAFs in vivo.

The tTAF proteins were concentrated in a particular subcompartment of the nucleolus in primary spermatocytes (Fig. 1). Expression of a functional green fluorescence protein (GFP)–tagged genomic *sa* rescuing transgene revealed that expression of Sa-GFP turned on specifically in male germ cells soon after initiation of spermatocyte differentiation and persisted throughout the remainder of the primary spermatocyte stage, disappearing as cells entered the first meiotic division (Fig. 1A). Some Sa-GFP was detected associated with condensing chromatin (arrowheads in Fig. 1, D and E). However, most Sa-GFP localized to the nucleolus (Fig. 1, C to E), in a pattern complementary with Fibrillarin, which

Departments of Developmental Biology and Genetics, Stanford University School of Medicine, Stanford, CA 94305–5329, USA.

*Present address: Department of Biological Science, Goucher College, Baltimore, MD 21204, USA.
†Present address: Biology Department, Massachusetts Institute of Technology, 77 Massachusetts Avenue, Cambridge, MA 04159, USA.
‡To whom correspondence should be addressed. Department of Developmental Biology, Beckman Center B300, 279 Campus Drive, Stanford University School of Medicine, Stanford, CA 94305–5329, USA. E-mail: fuller@cmgm.stanford.edu